Optical strain fields in shear and tensile testing of textile reinforcements

A. Willems, S.V. Lomov, I. Verpoest, D. Vandepitte

Optical strain fields in shear and tensile testing of textile reinforcements

A. Willems, S.V. Lomov, I. Verpoest, D. Vandepitte

PII: S0266-3538(07)00340-5
DOI: 10.1016/j.compscitech.2007.08.018
Reference: CSTE 3811

To appear in: *Composites Science and Technology*

Received Date: 21 May 2007
Revised Date: 20 August 2007
Accepted Date: 21 August 2007

Please cite this article as: Willems, A., Lomov, S.V., Verpoest, I., Vandepitte, D., Optical strain fields in shear and tensile testing of textile reinforcements, *Composites Science and Technology* (2007), doi: 10.1016/j.compscitech.2007.08.018

Optical strain fields in shear and tensile testing of textile reinforcements

A. Willems[a,*], S.V. Lomov[b], I. Verpoest[b] and D. Vandepitte[a]

[a] *Katholieke Universiteit Leuven, Department of Mechanical Engineering, Division PMA, Kasteelpark Arenberg 41, BE-3001 Heverlee*

[b] *Katholieke Universiteit Leuven, Department of Metallurgy and Materials Engineering, Kasteelpark Arenberg 43, BE-3001 Heverlee*

Abstract

This paper presents deformability tests on textile reinforcements in biaxial tension and shear using digital image correlation to calculate strain fields from in-plane images. Macro-scale strain fields (i.e. strain gauge length $\geq$ Repetitive Unit Cell) are applied to assess the reliability of loading conditions in tensile and shear tests, and to verify the assumption that the tensile state affects the shear resistance of a weave. Picture frame shear tests on a glass weave, a glass-PP weave and a carbon NCF are presented. The glass-PP weave is also tested in biaxial tension and in shear at three different tensile preloads. It is concluded that full-field optical techniques are essential to reliably assess the textile deformation and homogeneity of loading in textile testing. Significant tensile-shear interaction is observed. Nevertheless, further verification is recommended to assess the influence of uncontrolled yarn tensile load and the frame/fabric shear discrepancy on the empirical shear resistance.

Key words: Fabrics/Textiles, Mechanical Properties, Non-linear behaviour, Digital Image Correlation

PACS: A, B, B,

1 Introduction

Automated manufacturing of textile composite shell-like products typically requires draping of dry or pre-impregnated textile sheets. Large local deformations occur in the textile sheet in order to adapt to the curved shape. These deformations affect the local fibre directions, volume fractions, and thickness, i.e. factors that together with the consolidation level and the occurrence of flaws (e.g. wrinkling, tearing) determine the product quality. Simulation tools that link product quality to material, mold and process parameters are being developed to support design and process optimization [1–3]. The prediction of local deformations is an essential task within this objective. Mechanical models try to incorporate the mechanics of the textile into continuum-based or discrete 'macro-scale' material models and are generally implemented in a nonlinear FE code. A textile is a heterogeneous material, characterized by a repetitive textile structure, called 'Repetitive Unit Cell' (RUC). The mechanical properties of fabrics are highly nonlinear due to the deformation mechanisms at smaller scales. A multi-scale approach is thus required to build predictive models that link drape (macro scale) mechanics to deformations mechanisms at the scale of the RUC, called the 'meso scale', or lower scales.

Deformability characterization of (pre-impregnated) textiles provides vital data for the validation of meso-scale material models or the identification of empirical macro-scale models. Textile deformability testing mainly focuses on in-plane characteristics as shear resistance and biaxial tension. No stan-

dard test methods are available, though efforts were made to comprehend and compare shear test procedures [4–9]. Shear characterization receives the most attention because it is the most pronounced deformation mode during draping. The initial shear resistance is very low, as long as friction at the contact zones between yarn families is dominating. At larger shear angles, parallel yarns are jammed and a lateral compressive force is built up, leading to a steeply increasing resistance and contributing to out-of-plane wrinkling [10]. Two shear test methods are in vogue: a bias tensile test (i.e. a uniaxial tensile test with principal directions at +/- 45 degrees with regard to the tensile load) and a dedicated test in a shear fixture, called 'Picture Frame'. The bias test is easy to perform, but introduces an inhomogeneous deformation field, where the unconstrained fibres at the side edges may slip. The picture frame enforces almost pure shear, but careful fibre alignment with respect to the frame edges is crucial. It is assumed that the biaxial tensile state of a textile affects the shear resistance, because it alters the conditions of the yarn interaction (crimp, yarn compression, normal forces), and hence friction at the cross-sections. Numerical [11] and experimental efforts have been made to study the influence of pretension on the shear resistance [6,15] and wrinkling [12]. A pre-stressing device is used in [13,14], and prestressing bolts on the shear frame in [6,12,15]. In [12] it was observed for carbon and glass woven prepregs, that the onset of wrinkling could be increased by 5–20° when applying a tension of 20 Mpa (>20N/mm). In [6] picture frame tests on a dry weave with different (unspecified) levels of pretension did not alter shear resistance curves significantly, whereas in [15] a significant effect of pretension on shear resistance was demonstrated for three levels in the range of 0-20 N/yarn. Moreover, via force transducers perpendicular to the frame edges, a significant increase in yarn tension was measured throughout the shear test.

Biaxial tensile tests are used to characterize the nonlinear tensile stiffness in the principal material directions (i.e. warp/weft fibre directions for a weave and course/whale directions for a knit). Yarns are often crimped (i.e. curved due to the interlaced textile structure), and need to be straightened before actually being stretched. Hence the initial tensile stiffness is typically low, but increases highly once fibres are stretched. Other complex interactions occur during tension, like crimp exchange (i.e. exchange of waviness between different yarn families) and yarn compression at contact zones. Due to these deformation mechanisms the tensile behaviour in one yarn direction is affected by the load imposed in the other yarn direction. The biaxial test, first introduced by [16], further developped and applied by among others [17,18], imposes a tensile load in the two principal material directions of the fabric. Different biaxial loading paths are realized by varying the force ratio or the displacement ratio in both directions.

The digital image correlation technique (DIC) is an optical-numerical technique that provides quantitative and qualitative information on the heterogeneous deformation of an object. A CCD camera acquires grey scale images of an object during loading, and calculates a displacement field tangential to the object surface based on a comparison between the subsequent images. The DIC technique is of practical interest in the field of textile characterization due to its contactless nature and the possibility to tailor the strain gauge length to the material scale of interest. Macro-scale DIC (i.e. strain gauge length > RUC) is used in the picture frame test [9,19,20], in the bias test [21] and in the biaxial test [19,22]. [9] report shear deviations between the frame and the fabric (dry weaves) of 5 to 10° at 60 ° frame shear (or 8–16.7% error), [20] in the order of 2–4 ° at 30 ° frame shear. [9] demonstrates the different stages in shear deformation on a dry plain weave in meso-scale DIC (i.e. strain gauge

length < RUC). In the current paper the DIC technique is used to extract macro-scale textile deformations in tensile and shear tests of weaves (1) to verify the homogeneity of loading and compare the fabric deformation to the rig deformation, and (2) to verify the effect of the biaxial tensile state on the shear resistance.

2 Materials and test program

Three types of textile reinforcements have been studied (see [18,20]): 3 glass weaves, 3 glass-PP weaves (Twintex®) and 2 types of carbon non-crimp fabrics. This paper presents results on only one fabric per group (table 1) to illustrate overall trends. The glass-PP weaves are part of a woven benchmark exercise [8] and are heavier than the glass weaves. The glass-PP fabric RR2 is unbalanced as it has about 9.7 % crimp in the warp direction but only 0.1 % crimp in the weft direction. The crimp c characterizes the degree of out-of-plane waviness of a yarn, and is defined as $c = (L_{yarn} - L_{fabric})/L_{fabric} * 100$. Three kind of tests are presented: picture frame shear tests on the fabrics in table 1, picture frame shear tests with different biaxial pretension on the RR2 and uniaxial/biaxial tensile tests on the RR2. Two sample configurations are used in the shear tests: the 'Large Cross' for the regular shear tests and the 'Small Square' for the shear tests with pretension. Since current authors performed RR2 shear tests on two sample configurations, and other configurations were tested in the framework of the woven benchmark [7], the effect of the sample configuration and preload is also discussed.

3 Digital image correlation (DIC)

The DIC technique was developed in the 1980's and has since been improved and developed a lot. The basic principles are well described in [23]. The DIC technique requires a random speckle pattern, natural or artificial, attached to the material in order to track the local deformations. The grey scale images of an object during loading are compared with an image correlation software. First the displacement field is calculated tangential to the object surface, then the strains are derived from the displacement gradients. The displacement resolution is typically of sub-pixel accuracy ($\sim \frac{1}{50}$ of a pixel), and the maximum strain accuracy in the order of 0.02 %. The processing parameters are:

Subset window: To track the displacement of one particular point P, a neighbourhood area of pixels around P is needed as a template in the pattern-matching process. This neighbourhood, called 'subset window', is always a square array of pixels in commercial softwares. Because the subset is deformed between subsequent images, a first order photometric transformation is applied on the undeformed subset coordinates in order to obtain a good match in the subsequent image.

Step size: The step size is the distance (in pixels) between the centre points of neighbouring subsets, and determines thus the spatial resolution. To obtain a continuous displacement field the step size must be smaller than the subset size.

Strain window: The strain is calculated in strain windows, i.e. arrays of $p*p$ neighbouring subsets. The first order transformation in the undeformed coordinates (i.e. the deformation gradient $\underline{\underline{\mathbf{F}}}$) that best approximates the displacement field of the strain window is found, from which all strain measures

can be derived. The strain gauge length for a subset of $m * m$ pixels, a step size of n pixels and a strain window of $p * p$ subsets is $m + n(p - 1)$.

3.1 Special considerations in textile testing

Speckle pattern For the displacement mapping it is important to have enough grey scale gradients in all directions within a subset. Since the natural speckle pattern on a yarn consists mainly of parallel (fibre) lines (Fig. 1), little grey scale gradients are available along the fibre direction. Optical measurements using subsets smaller than a RUC (i.e. meso-scale) should thus be interpreted cautiously. An artificial speckle pattern can improve the DIC accuracy.

Lighting A diffuse light source reduces the noise contrast due to shadows and reflections that are related to the local normal direction of the wavy textile surface. Applying dust onto the surfaces helps to decrease the reflectivity.

Lenses and camera setup Textile deformability studies mainly focus on the in-plane shear and tensile behaviour, which makes 2D DIC a logical choice. While the out-of-plane deformation of the textile surface can be overcome by using a long distance focal lense, wrinkling makes 2D DIC impossible. 3D DIC on the other hand is problematic due to the surface waviness that creates shadows and variable reflections.

The reported 2D DIC measurements use a diffuse light source and some dust is applied to the surface. Only in the shear tests with pretension an additional grey speckle is applied.

3.2 Equipment and data processing

Two camera systems have been used with 16 mm and 50 mm lenses: the ARAMIS 768*572 pixel 12 bit gray scale CCD camera, and the LIMESS 1392*1040 pixel 12 bit gray scale CCD camera. The systems provide access to the major and minor strains, and the strains along the camera axes. However, in textile characterization and draping it is important to assess the shear angle γ (defined as $\gamma = \pi/2 - \alpha$, with α the angle enclosed between two fibre bundles), the 'material strains' along the fibre directions and the overall rotation of the material. These deformation measures can be derived from the deformation gradient $\underline{\underline{F}}$, which is not accessible in the LIMESS system.

The image magnification factors and DIC processing parameters, used in the tests, are summarized in table 2 and illustrated in Fig. 1. The angle between the camera axes and the weft fibres is 0 ° for the biaxial tests and 45 ° for the shear tests. The strain calculation is performed as follows:

$$\underline{x} = \underline{\underline{F}} \cdot \underline{X}; \underline{r} = \underline{a}, \underline{b}; \underline{X} = \underline{A}, \underline{B} \tag{1}$$

$$\lambda_x = \|\underline{x}\|, \epsilon_x = ln(\lambda_x) \tag{2}$$

$$\alpha_{fabric} = acos(\frac{\underline{a} \cdot \underline{b}}{\lambda_a \lambda_b}) \tag{3}$$

$$\gamma_{fabric} = \pi/2 - \alpha_{fabric} \tag{4}$$

$$\underline{\underline{R}} = \underline{\underline{F}} \cdot \underline{\underline{U}}^{-1}; \phi = acos(R_{11}) \tag{5}$$

Method 1: In **the shear test with(out) pretension** on the RR2, the textile strains are derived by a matlab routine that calculates the deformation gradient $\underline{\underline{\mathbf{F}}}$ from the displacement field of 3*3 subsets. A linear least-squares solution for the six parameters t_i and F_{ij} (i = 1,2) is obtained by minimizing the geometrical distance between the 'measured' new coordinates and the

'estimated' new coordinates. Two parameters t_i determine the rigid body translation, and the other four, F_{ij}, the components of the deformation tensor in the global frame. The logarithmic fibre strains ϵ_a, ϵ_b, the shear angle γ and the rigid body rotation ϕ of the material are calculated from $\underline{\underline{\mathbf{F}}}$ as in equations 1 to 5. $\underline{\mathbf{A}}$ and $\underline{\mathbf{B}}$ represent unit vectors in the fibre directions in the reference state, $\underline{\mathbf{a}}$ and $\underline{\mathbf{b}}$ the corresponding deformed vectors.

Method 2: In the **biaxial test** the fibre strains ϵ_a, ϵ_b are directly provided by ARAMIS.

Method 3: In the **shear tests** on the three fabrics in 'Large Cross' setup, the deformed coordinates ($\underline{x}$) of 2*2 neighbouring subsets are combined to calculate the fibre strains and enclosed angle α (see Fig. 2). Since the diagonals of this strain window are initially aligned with the fibres (see grey lines in Fig. 2), the angle α can be calculated by applying the cosine rule.

4 Shear tests

4.1 Picture frame

Fig. 3a depicts a sketch of the picture frame. The frame is mounted in a universal tensile machine via the vertical bar that is connected to joint E. Joint A is attached to the ground plate and joint D can freely slide in the groove of the vertical bar when the frame deforms. The force is registered by a 1 kN load cell. Shearing an empty frame provides a calibration force-displacement curve, which reflects the gravitational forces of the frame and possible frictional resistance. However, for this rig it was verified both experimentally and via a kinematic-dynamic model that friction is negligible for the tests performed.

The calibration curve is subtracted from each textile force-displacement curve to obtain only the force component due to the textile deformation. The kinematic relation between the shear angle γ of the frame (with $\gamma = \pi/2 - \alpha$, see Fig. 3a) and the cross-head displacement (i.e. displacement of joint E) is derived analytically and approximated by a third order polynomial for convenience:

$$\gamma[deg] = 2.73e^{-4}x^3 - 2.91e^{-2}x^2 + 2.773x[mm], \tag{6}$$

4.2 Test configurations

Various sample configurations and clamping conditions are being used in the picture frame test, differing in frame length, ratio of fabric length to frame length and the type of arm parts – applicable to weaves – i.e. with or without loose yarns removed. Fig. 3b and c illustrates the two sample configurations used in this study.

- Large Cross

  This test setup is fully described in [20], and corresponds to Fig. 3c. Cross-shaped samples with a fabric length of 176 mm are cut and clamped into the corrugated grips. The corrugated clamps apply a fabric-dependent pretension to the sample, estimated in the range 0.2-0.5% strain. On each sample three shear cycles are performed at a constant speed of 20 mm/min. At least 5 repeats have been undertaken.

- Small Square

  This configuration is used in the shear tests with pretension on the RR2. Three biaxial tensile preloads are applied in warp/weft direction: 0.27/0.27, 1.36/2.01, 3.27/5.03 N/mm. Tabs for the biaxial preloading are prepared via

local consolidation of the textile (Fig. 4a). Then the sample is cut to 30 weft and 14 warp yarns (fabric length of 74 mm) and loose yarns in the arm parts are removed. This sample configuration is shown in Fig. 3b. Then the textile is loaded in tension in the biaxial tensile machine (Fig. 4b). Next the textile is clamped into the picture frame, that is locked in its square reference position. Flat serrated grips clamp the textile in the frame after 0.5 mm thick rubber sheets are stacked above and below the yarns to obtain an even load distribution and avoid fibre breakage. Finally the picture frame is installed into a universal tensile machine, the lock is released and the shear test is performed (Fig. 4c). Five shear cycles are measured at a constant speed of 5–10 mm/min. For each test condition 4 to 5 repeats have been undertaken.

4.3 Shear force calculation

The shear force (see Fig. 3a) is usually calculated directly from the cross-head force, assuming that all the mechanical work is dissipated as shear deformation energy and that the fabric shear γ_w is equal to the frame shear γ_f. Under these assumptions the shear force is calculated as:

$$F_{shear}[N] = \frac{\tilde{F}_D}{2cos(\alpha/2)} = \frac{\dot{y}_E/\dot{y}_D F_E}{2cos(\alpha/2)} \tag{7}$$

with α is the kinematic angle of the frame. For simplification of expressions the mechanical equivalent loading case is considered where the external force $\tilde{F}_D$ is applied on joint D (Fig. 3a) instead of on joint E. The velocity ratio $\dot{y}_E/\dot{y}_D$ is derived analytically and approximated as:

$$\dot{y}_E/\dot{y}_D = 7.739e^{-6}y_E^3 - 5.468e^{-6}y_E^2 + 6.921e^{-3}y_E + 0.113[mm] \tag{8}$$

The shear force per fabric width, is calculated as outlined in [5] in the assumption that only the fabric dissipates energy and not the arm parts:

$$F_{shear}[N/mm] = \frac{\tilde{F}_D}{2cos(\alpha/2)} \cdot \frac{L_{frame}}{{L_{fabric}}^2} \tag{9}$$

Though in the 'Cross' sample the arm parts may also have a contribute to the internal energy, this is not considered at present.

4.4 Homogeneity of loading

The deformation field is calculated in a region of interest (ROI) somewhat smaller than the square centre of the samples (Fig. 5a and c). Fig. 5b and c illustrate the textile deformation during the shear test. The homogeneity of the shear field is illustrated in Fig. 6 on the RR2 for both configurations at 34.5° mean fabric shear. The homogeneity of deformation is reasonable as long as no severe wrinkling is present. Beyond severe wrinkling the assumption of in-plane deformation is not valid anymore, and 2D DIC is no longer reliable. Nevertheless the DIC technique can be used to quantify the inhomogeneity due to out-of-plane wrinkling. The 'Large Cross' has larger scatter, attributed to the wrinkling, that starts between 16 - 38° frame shear, while in the 'Small Square' test no wrinkling occurs (compare Fig. 6b with Fig. 6a). As wrinkling is an instability phenomenon governed by the tensile, in-plane shear and out-of-plane bending stiffness, the occurrence of wrinkling in forming can not be related to one particular shear locking angle. Analogous in the shear test wrinkling is likely to occur sooner the larger the fabric to frame length ratio and the less membrane tension [12].

4.5 Fabric deformation – 'Large Cross'

Fig. 7 shows the difference between the fabric and the frame shear angle for the three textiles. The strain processing for R580 and B2 is method 3, also used in [20], whereas for RR2 this is method 1 (see section 3.2). The error-bars indicate the standard deviation over the ROI. The fabric deformations are representative of respectively normal weaves (R580), heavy/tight weaves (RR2) and NCF's (B2). All fabrics, with exception of the heavy/tight glass-PP weaves (RR1 and RR2), typically have a textile shear deformation lower than the frame shear. It seems that the local yarn bending at the frame edges counteracts the 'lagging angle' (Fig. 3a) between the textile and the frame for the heavy weaves. The larger the in-plane bending stiffness of the arm parts (large yarn linear density, tight structure, no loose yarns removed,...) the more pronounced the local yarn bending will be. Shear deviations become as large as 6–8% for these textiles . Once the textiles start to wrinkle severely the shear difference curve suddenly drops (noticeable drop around 40°) , indicating that the DIC results are no longer reliable.

4.6 Fabric deformation in RR2 – 'Small Square' versus 'Large Cross'

Fig. 7c depicts also the difference between the textile and the frame shear for the RR2 in the 'Small Square' configuration. The textile shear deformation in the 'Small Square' configuration is not affected by the biaxial tensile state of the fabric, and thus one curve represents the three different tensile conditions. The errorbars, representing the standard deviation, indicate little variability between individual tests. In the 'Small Square' configuration, the fabric shear

tends to be smaller than the frame shear deformation, whereas an opposite trend was found for the 'Large Cross' test on the same fabric. The different tendency can be explained by the fact that a small lagging angle (i.e. fabric shear lower than frame shear) is expected for the 'Square' configuration where the fabric centre is attached to the frame by ideal springs. In reality, however, local yarn bending occurs at the frame edges, an effect that is more pronounced for 'stiffer' arm parts (i.e. loose yarns not removed, see Fig. 5c), and may lead to a fabric shear that is larger than the frame shear. The frame to fabric shear deviation in the 'Small Square' test is about 7% at 37° and 12% at 50° frame shear, compared to 6% at 37° for the 'Large Cross'.

The rigid body rotation ϕ of the weave centre was assessed for the both configurations in the second shear cycle (Fig. 8a). A small clockwise rotation (in the order of 0.65 °) occurs during shear loading. The rotation is attributed to the unbalanced character of the weave. The rigid body rotation was also assessed for the 'Small Square' configuration between the reference positions of subsequent cycles, using the first image of cycle 1 as the undeformed reference (Fig. 8c). Small monotonous rotations occur between subsequent cycles in the order of 0.1-0.15°. Macro-scale material strains in the fibre directions are calculated for the reference states of subsequent shear cycles, using the first image of cycle 1 as the undeformed reference. A monotonous increase in fibre strain is assessed between subsequent cycles in the order of 0.3–0.9% warp strain. However, from visual observation it is clear that these are not actual strains, but a result of sideways sliding of the yarns during the shear deformation that is not recovered during un-shearing (see arrows in Fig. 5a). In the 'Large Cross' test the 'apparent' strains between subsequent cycles are smaller, in the order of 0.35% and 0.1% in weft respectively warp direction. This is logical because yarn sliding is hindered more by neighbouring yarn

cross-sections in the 'Cross' sample.

4.7 Shear resistance

In the 'Small Square' test with pretension the shear resistance curves shift downward during the first 3 to 4 cycles, whereafter a stabilization occurs (Fig. 9). This well-known hysteresis phenomenon was reported before, among others in [6,13,20], and is caused by frictional energy dissipation in the material. For some samples additional cycles are measured after manually restoring the yarns that had slipped in their original position. These additional cycles fairly approximate the second cycle above 15° or lie in between the second and third cycle (see Fig. 9b), thus no relaxation nor fibre breakage occurs during shearing. Therefore the second cycle is believed to be most representative of the textile shear resistance, as suggested in [20], and will be used further in the material characterization. The more fabric tensile load the larger the force shift in subsequent shear curves (compare Fig. 9a and b), i.e. the more pronounced the hysteresis effect. This can be understood by the fact that the internal friction is directly linked to the tensile state in the fabric.

4.7.1 Tensile-shear interaction

The shear resistance can be expressed as shear force against textile shear or frame shear angle. Fig. 10a illustrates that the choice of the shear angle in the abscissa has a significant influence on the corresponding shear resistance curve. Fig. 10b shows the shear resistance for the three tensile loading conditions as shear force per textile shear angle. The data variability is large, because the test is ill-conditioned with respect to small yarn misalignments. This is

illustrated by the errorbars, that represent the standard deviation. Generally a rise in shear resistance is observed when the tensile load is increased, above 12 ° shear. Assuming a t-distribution for the shear force at a particular shear angle, one can say with 95% confidence that batch 3 (highest tension) has a higher resistance than batch 1 (lowest tension) in the range 14-42° and with 85% confidence that batch 2 has a higher resistance than batch 1 in the range 24-42°. This shear range corresponds to the phase in the shear deformation where friction between the cross-overs plays a major role, hence also the yarn tensile load. However, it is currently undetermined to what extend the frame/fabric shear deviation and the uncontrolled yarn tension during the shear deformation affects the empirical shear resistance. Further tests with an improved force measurement on the picture frame (as in [15]) are required to quantify the influence of the changing yarn tensile load and orientation.

4.7.2 Inter-lab variability

Fig. 11 shows the shear resistance curves for the RR2, measured by different labs in the framework of the woven benchmark exercise [8,24]. All curves have frame shear in the abscissa, except for the Small Square curves marked with 'DIC' that have fabric shear in the abscissa. Table 3 summarizes the sample configuration and applied tensile lpreoad of the tests. The shear force was calculated by formula 9. The tensile state for the UML test is unknown, whereas the tension in the UT and KUL76 test is estimated by the K.U.Leuven based on the low-stiffness part of the tensile curve, and the tensile strains (0.2–0.5%), assessed via lines applied onto the textile.

The inter-lab variability is quite large despite careful yarn placement and ef-

forts to enhance repeatability. Nevertheless the shear resistance for the 'Small Square' is in between the shear resistance of UML. Although the UT and KUL176 test use a similar frame and clamping method (UML removes a few loose yarns to avoid wrinkling), the curves do not coincide. The tensile-shear interaction observed in this study is of the same order as the inter-lab variability. The authors believe that the magnitude of tensile load combined with the shear discrepancy between the frame and textile (which is related to the sample configuration) is a major factor of the inter-lab variability. A bias test, performed by UT, is also presented in the graph. Picture frame tests measure higher shear resistance than the bias tests (see 'UT bias' in Fig. 11) because yarns can freely slide in the centre of a bias sample – i.e. no yarn tensile load can build up – contrary to the picture frame test. The bias test will thus underestimate the shear resistance, whereas the picture frame may be overestimating the resistance.

5 Biaxial tests

5.1 Equipment

The biaxial tensile machine at the K.U.Leuven (Fig. 12) is designed especially for testing textiles, films and thin sheets. The machine is composed of four axes, placed pairwise in two perpendicular directions. Each axis is actuated by a DC motor, that is mounted to a ball-screw spindle via a torsion coupling. The force is registered by force transducers with a maximum load capacity of 10 kN and accuracy of 0.1 %. Currently the axes are velocity controlled to move with constant speed, to a maximum of 175 mm/min. Because the speed

can be chosen freely in both directions, various biaxial loading cases can be achieved. The strains in the fibre directions are measured both with DIC in the centre of the sample (Fig. 12b), and between the clamps of the biaxial tester via laser distance sensors. Typically different stress-strain curves are derived in warp and weft direction at different warp-to-weft velocity ratios.

5.2 Test conditions

Tensile tests have been performed on fabric RR2 with a velocity ratio of 1/1 and 1/free (i.e. a uniaxial warp test), and a warp velocity of 6–60 mm/min. The tests with 6 and 60 mm/min were processed together, since no significant influence of velocity on tensile resistance was found. For every test condition, three to four repeats have been undertaken. Cross-shaped specimens are prepared with 28 warp and 14 weft yarns, covering an area of $68 * 73$ mm (Fig. 12a). In all tests the loose yarns in the arm parts are removed ('Square' samples), except for one 1/1 test ('Cross' sample). Tabs are prepared by local consolidation. The reference state is not easy to determine because of the low initial stiffness and the influence of gravity. In these tests the reference state was defined at a tensile load of 20 N in both directions (i.e. 0.3 N/mm or 0.7 $N/yarn$ in warp direction). This preload is higher than the 0.1 $N/yarn$, used in [22], but was chosen to enhance repeatability. The estimated absolute error in the strain measurement is in the order of 0.3% in weft and -0.7% in warp direction.

5.3 Homogeneity of the strain field

A typical strain field of the dilatational strain $\epsilon_{xx} + \epsilon_{eyy}$ is shown in Fig. 13 for velocity ratio 1/1 at an average value of 3.4%. The strain gauge length is about 6 mm, thus smaller than the RUC (RUC size of 10*20 mm). At the borders of the field (outside the dotted box) large deviations of the mean value occur due to side effects as outward sliding of yarns. Therefore only values inside the dotted box are used for the strain averaging. Since the subset windows are somewhat smaller than the unit cell, meso-scale deformations are qualitatively visible as well, as demonstrated by the fabric pattern (diagonals of cross-overs) being recognizable in the strain field.

5.4 Discrepancy between fabric and rig deformation

Fig. 14 shows the strain paths for the 1/1 tests in both sample configurations, measured on the fabric ('DIC') and enforced over the rig ('rig'). This graph clearly illustrates that the fabric deformation should be measured optically over the fabric central area, since the displacement of the clamps is not representative of the fabric deformation. Reason is that the compliance of the unidirectional arm parts and the fabric weave is of the same order. Consequently the fabric velocity ratio (or strain ratio) deviates from the enforced velocity ratio, due to the unbalanced fabric structure or unsymmetrical loading. The 'Cross' samples show larger deviations in velocity ratio than the 'Square' samples and have a variable fabric strain ratio during the 1/1 test.

Fig. 15 depicts biaxial force-strain curves in warp and weft yarn directions for the uniaxial and 1/1 test on the 'Square' sample. The curves marked

with 'DIC' are based on fabric strains, whereas the curves marked with 'rig' represent the enforced strains. The yarn tensile curves are also represented to serve as a reference for the amount of crimp exchange. When applying tension to yarns that are crimped (i.e. curved due to the weave structure) the yarns need to be straightened before actually being stretched. The degree of initial crimp and the warp/weft force ratio affect thus the amount of crimp exchange, visible in the nonlinearity of the curves. The large initial warp crimp (9.7%) explains why the low-stiffness part of the warp tensile curves is larger in comparison to the yarn curve. Compared to the uniaxial test it is logical that in the 1/1 test the low-stiffness part shortens in warp and lengthens in weft direction. The more weft tension, the more warp yarns will be prevented from fully de-crimping. A similar reasoning holds for the weft yarns, though weft yarns are much less crimped (about 0.1%). In the weft curve of the 1/1 test there is less tensile non-linearity compared to the 'unidirectional' yarn curve, since the straightening of the warp yarn actually causes some rise in the weft crimp. The strain deviations between the fabric and the rig are clearly visible in the force-strain curves, especially in the warp direction, due to the high initial crimp.

6 Conclusion

The DIC technique was used in shear and uniaxial/biaxial tensile testing of textiles 1) to assess the homogeneity of loading and the correspondence between the fabric and rig deformation, and 2) to assess the influence of the biaxial tensile state on the shear deformation and resistance in the picture frame test. Finally, the influence of sample configuration and pretension in

the picture frame test on the variability in shear resistance is illustrated on an unbalanced weave (RR2) and discussed. The main conclusions are as follows:

DIC in textile testing Full-field optical techniques are essential to reliably assess the textile strains (shear angle, fibre strains,...) and the homogeneity of loading. In the picture frame test the shear angle difference between the fabric and frame may become significant, depending on the fabric type. and the sample configuration. The shear angle difference between the fabric and the frame is not affected by the amount of tensile preload. In general the frame shear exceeds the fabric shear deformation. However, in heavy weaves with 'Cross' setup, the textile shear can exceed the frame shear, because the local yarn bending at the frame edges is the more pronounced the larger the in-plane bending stiffness of the arm parts. Some sideways yarn sliding is observed during the shear deformation, and is most pronounced when yarns are removed in the arm parts (i.e. 'Square' setup). An overall rigid body rotation of the weave centre (up to 0.65°) takes place and is attributed to the unbalanced character of the textile. In biaxial tensile tests the deformation and the velocity ratio of the fabric differs significantly from that enforced by the clamps due to the compliance of the arm parts. Samples with loose yarns removed in the arm parts have a more constant fabric velocity ratio.

Tensile-shear interaction and the picture frame test The picture frame shear test is ill-conditioned, since small yarn misalignments lead to large data variability. Nevertheless, a significant increase in shear resistance is found with increasing tensile load beyond a shear angle of 12°. However, it should be verified that the empirical tensile-shear interaction is significantly affected by the shear angle deviation between the fabric and the frame, combined with an uncontrolled yarn tensile load. Better control and/or mea-

surement of the tensile load in the picture frame test seems a necessary step towards more adequate investigation of the shear resistance, the tensile-shear interaction and the occurrence of wrinkling.

Variability in the picture frame test A large variability in the shear resistance of textiles was demonstrated when different sample configurations or clamping methods are used. The authors believe that the magnitude of tensile load combined with the shear discrepancy between frame and textile is a major factor of the inter-lab variability. Textile engineers will have to handle this uncertainty in their material models and drape simulations.

Any attempt to optimize the sample configuration should aim at minimizing both the 'out-of-plane wrinkling' and the shear deviation between the rig and the textile (which may lead to increasing yarn tension). Optimization seems quite cumbersome, however, due to the dependency on the textile structure, and the fact that local yarn bending at the frame edges cannot be prevented. A pragmatic suggestion is to make the arm parts as small as feasible, and remove just enough loose yarns – preferably at the grip zone – to reduce both out-of-plane wrinkling and local yarn bending.

Acknowledgements

We would like to thank the Fund for Scientific Research Flanders (FWO Vlaanderen) for funding this research.

References

[1] A.C. Long. *Design and Manufacture of textile composites*. Woodhead Publishing Limited, in association with The Textile Institute, 2005.

[2] A.C. Long. *Composites forming technologies*. Woodhead Publishing Limited, 2007.

[3] P. Boisse, R. Akkerman, J. Cao, J. Chen, S.V. Lomov, and A.C. Long. Composites forming. In F. Chinesta and E. Cueto, editors, *Advances in material forming. Esaform 10 years on*, pages 61–80. Springer, 2007.

[4] P. Harrison, M.J. Clifford, and A.C. Long. Shear characterization of viscous woven textile composites: a comparison between picture frame and bias extension experiments. *Composites Science and Technology*, 64(10-11):1453–1465, 2004.

[5] X. Peng, J. Cao, J. Chen, P. Xue, D. Lussier, and L. Liu. Experimental and numerical analysis on normalization of picture frame tests for composite materials. *Composites Science and Technology*, 64:11–21, 2004.

[6] D. Lussier. *Shear characterization of textile composite formability*. PhD thesis, University of Massachusetts at Lowell, 2002.

[7] J. Cao, H.S. Cheng, T.X. Yu, B. Zhu, X.M. Tao, S.V. Lomov, T. Stoilova, I. Verpoest, P. Boisse, J. Launey, G. Hivet, L. Liu, J. Chen, E.F. de Graaf, and R. Akkerman. A cooperative benchmark effort on testing of woven composites. In *proceedings ESAFORM 7, 2004*, 2004.

[8] www.gtwebsolutions.com/nwbenchmark/index.php.

[9] F. Dumont, G. Hivet, R. Rotinat, J. Launay, P. Boisse, and P. Vacher. Mesures de champs pour des essais de cisaillement sur des renforts tisses.

field measurements for shear tests on woven reinforcements. *Mecanique and Industries*, 4(6):627–635, 2003.

[10] J.W.S. Hearle, J. Amirbayat, and J.J. Twaites. *Mechanics of flexible fibre assemblies*. Sijthoff and Nordhof, 1980.

[11] S.V. Lomov and I. Verpoest. Model of shear of woven fabric and parametric description of shear resistance of glass woven reinforcements. *Composites Science and Technology*, 66(7-8):919–933, 2006.

[12] U. Breuer, M. Neitzel, V. Ketzer, and R. Reinicke. Deep-drawing of fabric-reinforced thermoplastics: wrinkle formation and their reduction. *Polymer Composites*, 17(4):643–647, 1996.

[13] M.F. Culpin. The shearing of fabrics: a novel approach. *Journal of the Textile Institute*, 70(3):81–87, 1979.

[14] B. J. Souter. *Effects of fibre architecture on formability of textile preforms*. PhD thesis, University of Nottingham, 2001.

[15] J. Launay, G. Hivet, A.V. Duong, and P. Boisse. Experimental analysis of the influence of tensions on in plane shear behaviour of woven composite reinforcements. *Composites Science and Technology*, In Press, Corrected Proof, 2007.

[16] S. Kawabata, M. Niwa, and H. Kawai. Finite-deformation theory of plain-weave fabrics .1. biaxial-deformation theory. *Journal of the Textile Institute*, 64(1):21–46, 1973.

[17] K. Buet and P.Boisse. Experimental analysis and modeling of biaxial mechanical behavior of woven composite reinforcements. *Experimental Mechanics*, 41(3):260–269, 2001.

[18] S.V. Lomov, M. Barburski, T. Stoilova, I. Verpoest, R. Akkerman, R. Loendersloot, and R.H.W. ten Thije. Carbon composites based on

multiaxial multiply stitched preforms. part 3: Biaxial tension, picture frame and compression tests of the preforms. *Composites Part A-Applied Science and Manufacturing*, 36(9):1188–1206, 2005.

[19] A. Willems, S.V. Lomov, Z. Yingbo, I. Verpoest, and D. Vandepitte. Deformability characterization of fabrics using large and small scale full field optical strain measurements. In *proceedings of the ECCM 12 Conference*, 2006.

[20] S.V. Lomov, A. Willems, I. Verpoest, Y. Zhu, M. Barburski, and T. Sotilova. Picture frame test of woven composite reinforcements with a full-field strain registration. *Textile Research Journal*, 76(3):243–252, 2006.

[21] P. Potluri, D.A.P. Ciurezu, and R.B. Rarngulam. Measurement of meso-scale shear deformations for modelling textile composites. *Composites Part A-Applied Science and Manufacturing*, 37(2):303–314, 2006.

[22] P. Boisse, M. Borr, K. Buet, and A. Cherouat. Finite element simulations of textile composite forming including the biaxial fabric behaviour. *Composites Part B: engineering*, 28(4):453–464, 1997.

[23] M.A. Sutton, W.J. Wolters, W.H. Peters, W.F. Ranson, and S.R. McNeill. Determination of displacements using an improved digital correlation method. *Image and Vision Computing*, 1(3):133–139, 1983.

[24] www.mech.northwestern.edu/ampl/benchmark/.

Fig. 1. Typical subset and strain windows on the RR2 fabric for the shear test with pretension, and tensile tests

Fig. 2. The initial ($\underline{X}$) and deformed ($\underline{x}$) coordinates of 2-by-2 neighbouring subset windows. If the fibres are aligned with the diagonals (grey lines) in the reference state, the diagonals in the deformed state should follow the fibre directions

Fig. 3. (a) Sketch of the picture frame. The frame deformation is enforced by the displacement of joint E. The crosshead force and shear force are indicated, (b) 'Small Square' setup for shear tests with pretension. The weave length is 74 mm, and loose yarns are removed, (c) 'Large Cross' setup with corrugated grips. The weave length is 176 mm, and loose yarns are not removed

Fig. 4. a) Sample preparation through local consolidation in a hand press, b) Clamping of sample in picture frame after preloading in biaxial tester, c) Picture frame test with CCD camera perpendicular to the fabric

Fig. 5. Picture frame test: a) 'Small Square' setup in reference state after the first shear cycle. The ROI and subset window are indicated. Some sideways yarn sliding is visible at the edges of the fabric centre, b) Fabric deformation for the 'Small Square' setup, c) Fabric deformation for the 'Large Cross' setup. Local yarn bending at the edges is more pronounced in this configuration

Fig. 6. Shear angle field in degree at 34.5° fabric shear. a) for the 'Small Square' setup, b) for the 'Large Cross' setup

Fig. 7. Difference between the fabric and the frame shear for three fabric types. a) and b) 'Large Cross' setup and strain calculation method 1 (section 3.2), c) 'Large Cross' and 'Small Square' setup and strain calculation method 1 (section 3.2)

Fig. 8. a) Rigid body rotation in shear test with pretension, derived by strain calculation method 1 (section 3.2) a) during the second shear cycle on tests with lowest tensile preload , c) between reference states of subsequent cycles for the three biaxial tensile states

Fig. 9. Typical shear resistance curves. a) for fabric with low tension (batch 1), b) for fabric with high tension (batch 3). '6*' and '7*' indicate shear curves, registered after manually restoring the yarns in their initial position

Fig. 10. Shear resistance in second cycle: a) for test with low tension (batch 1). The full line uses the fabric shear as abscissa, the dotted line frame shear, b) for all tensile states against fabric shear

Fig. 11. Comparison of shear curves on RR2, performed by various labs in the framework of a woven benchmark [8,24]. The legend lists the group and the size of the weave centre. 'KUL' indicates results of the present authors. The frame shear is used as abscissa, unless the curve is marked with 'DIC'

Fig. 12. (a) Cross-shaped fabric sample and approximate dimensions, (b) Biaxial tensile machine with CCD camera installed

Fig. 13. In-plane dilatational strain field $\epsilon_{xx} + \epsilon_{yy}$ for test with velocity ratio 1/1 at an average strain value of 3.4% and strain window of about 6 mm. Subsequent data processing uses only the area in the dotted box

Fig. 14. The strain paths for the 1/1 tests, of the fabric weave, measured optically ('DIC'), and enforced over the rig ('rig'). The two sample configurations are indicated by 'Square': yarns removed in the arm parts, and 'Cross': without yarns removed

Fig. 15. Tensile curves in warp respectively weft yarn direction. Curves marked with 'DIC' use strains based on optical measurements, whereas the curves marked with 'rig' use enforced strain over the biaxial test rig

Table 1
Three fabric types

Fabric ID	R580	TPECU44 (RR2)	B2
Pattern	plain weave	twill 2/2	NCF
Fibres	glass	glass/PP	carbon/PES[1]
Yarn linear density tex	1200/1200	1870/3740	7.6[1]
Ends/picks $yarns/cm$	2.3/2.3	4.1/1.9	–
Areal density g/m^2	580	1485	329
Stitch spacing mm	–	–	5.0×2.6
Stitch pattern	–	–	tricot-chain

[1]: stitch parameter

Table 2
Parameters in DIC image processing

	Biaxial	Shear	Shear on RR2 'Cross'/'Square'
System	ARAMIS	ARAMIS	ARAMIS/LIMESS
Magnification factor [pix/mm]	3.5–7	1.4	5–6
Strain calculation method	method 2	method 3	method 1
Subset size [mm]	2.5–10	9.5	14
Step size [mm]	2–8	8	2.5
Strain size [subset*subset]	3*3	2*2	3*3
Strain gauge length [mm]	6–28	18	19

Table 3
Summary of test configurations

	KUL176 Large Cross	KUL74 Small Square	UT180	UML140	UML98
L_{frame}, mm	250	250	250	216	216
L_{fabric}, mm	176	74	180	140	98
L_{fabric}/L_{frame}	0.7	0.3	0.72	0.65	0.45
tension, N/mm	$< 0.3^{(1)}$	$0.3/1.7/4^{(2)}$	$< 0.3^{(1)}$	–	–
clamps	corrugated	flat	corrugated	flat	flat
yarns removed	no	yes	a few	no	no

(1): Estimation based on linearized low-stiffness curve, and strain of 0.2–0.5%
(2): Average of warp and weft tension for batch 1/2/3 in shear tests with pretension

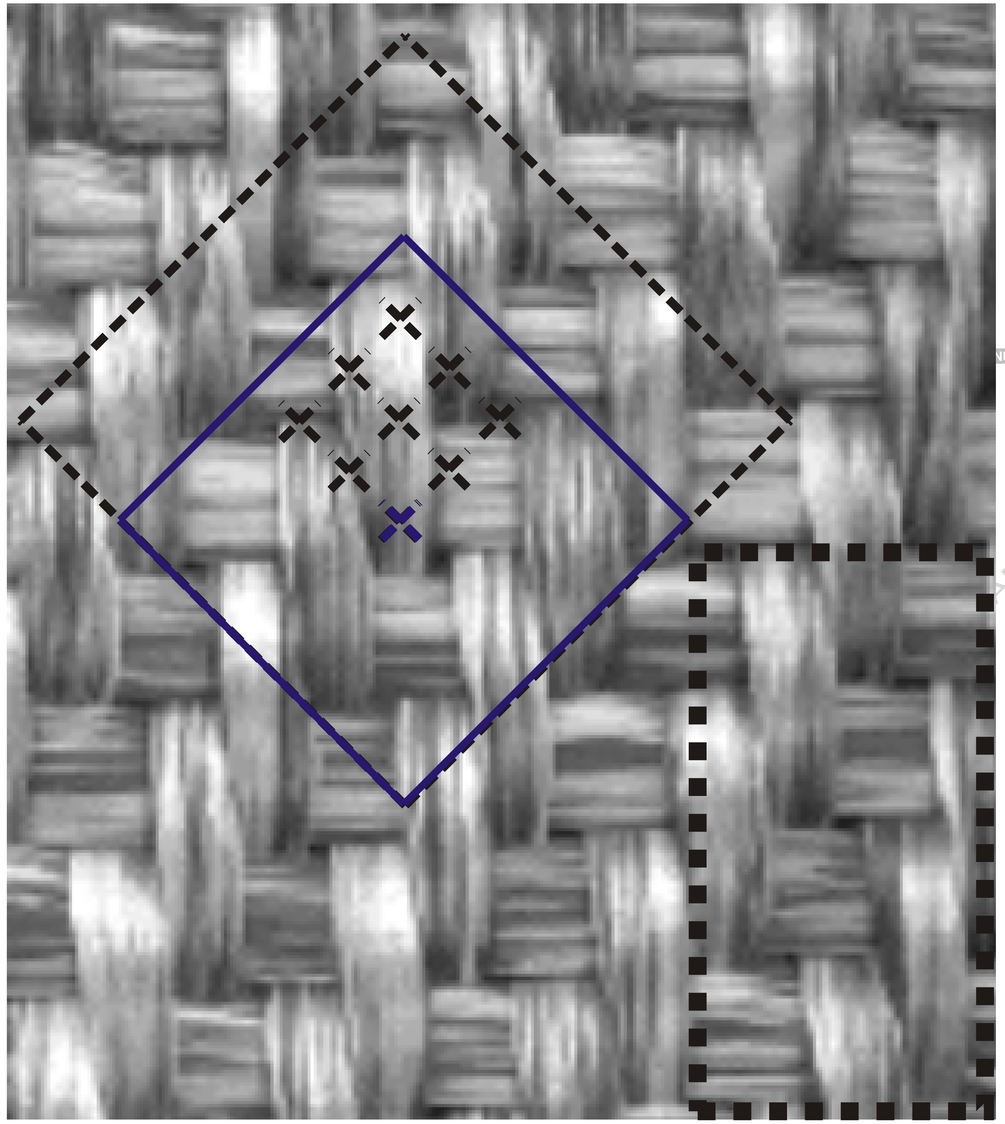

Subset window

Strain window

Unit cell

3*3 subset

Y X

Shear with pretension

10 mm

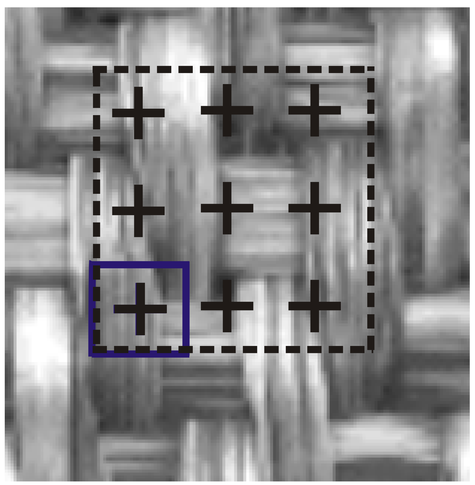

Y X

Biaxial test

WARP

WEFT

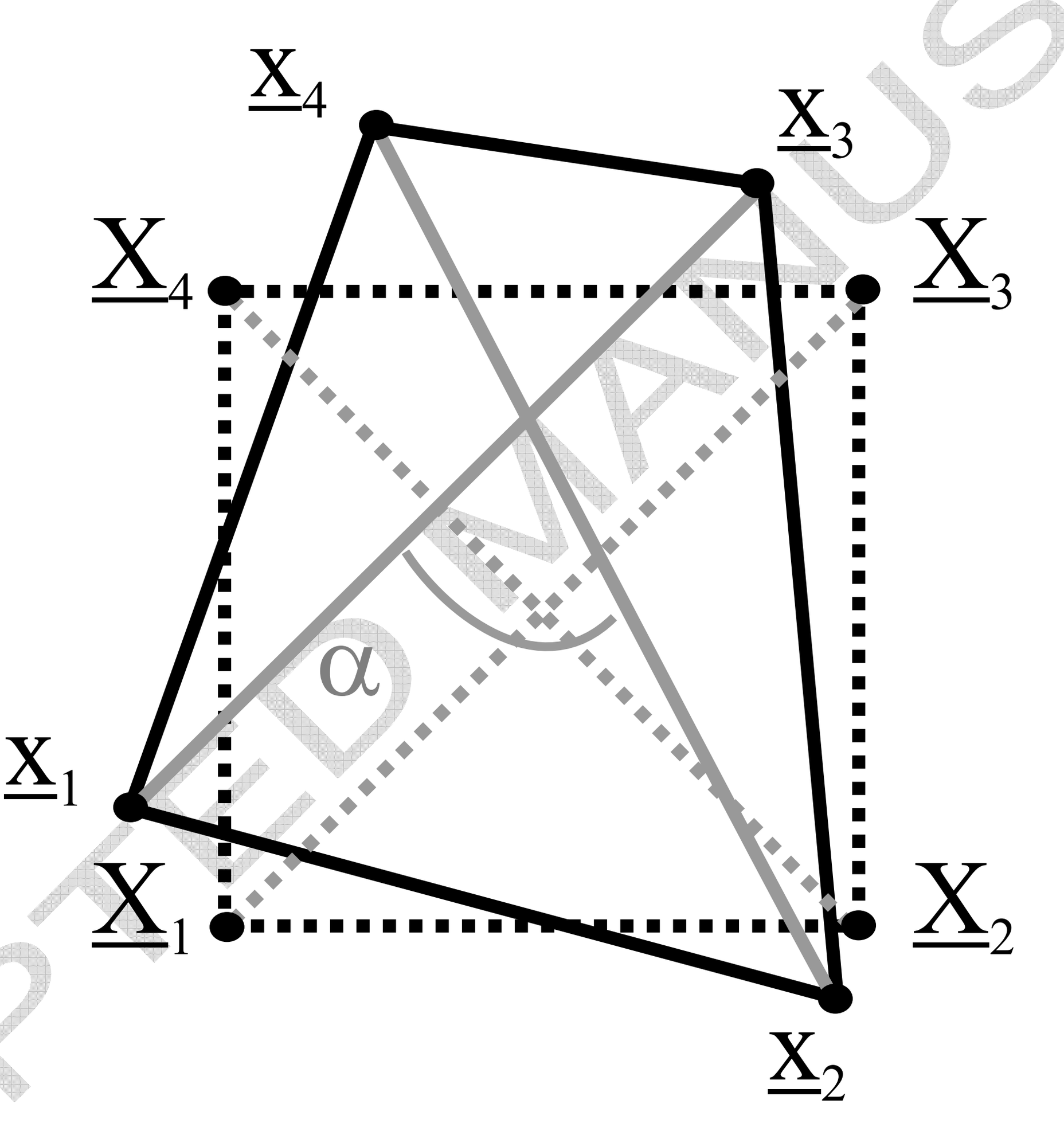
X4
X3
X4
X3
α
X1
X1
X2
X2

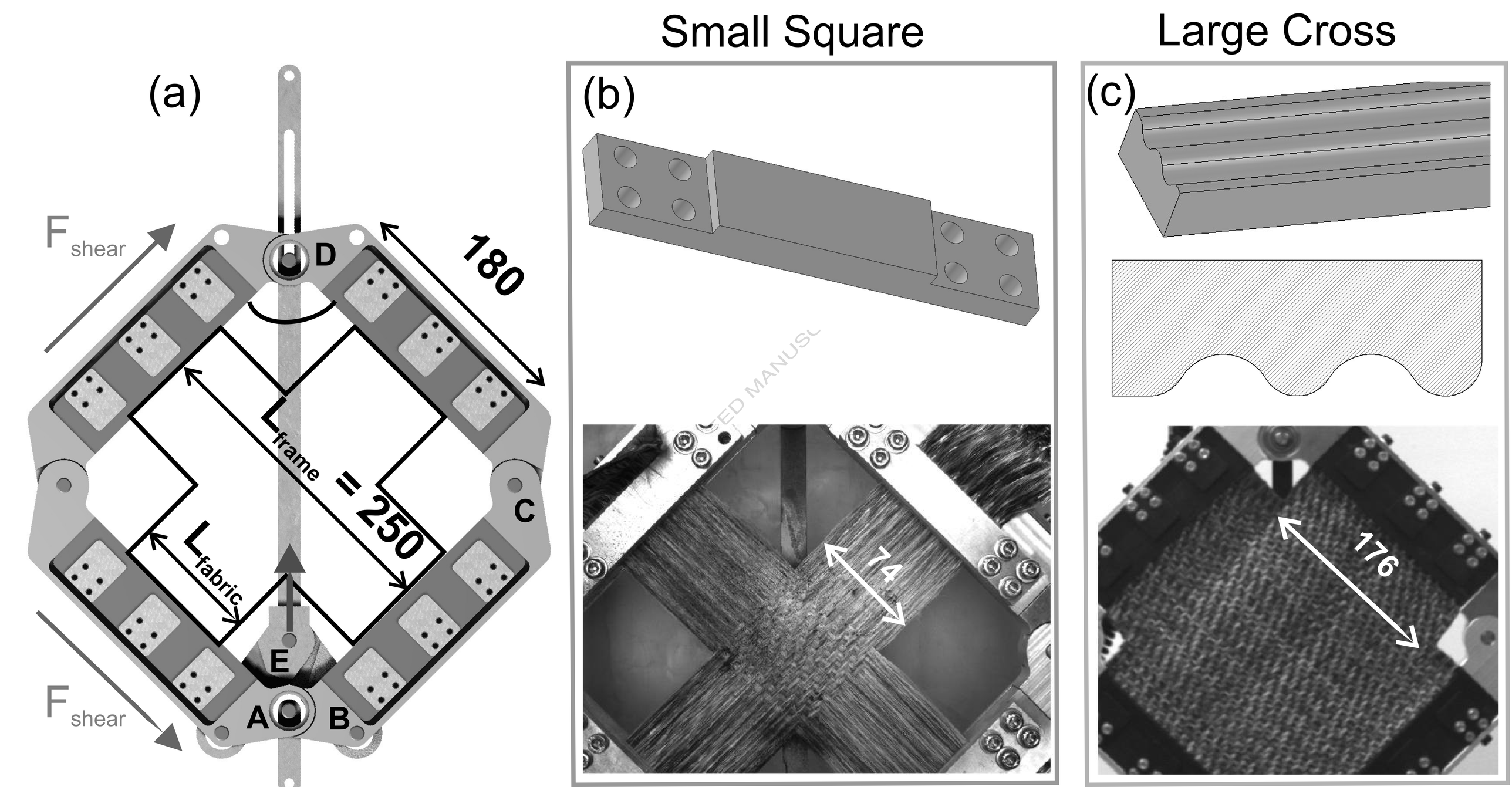
Small Square
Large Cross
(a)
(b)
(c)
F shear
F shear
D
C
E
A
B
180
L frame = 250
L fabric
74
176

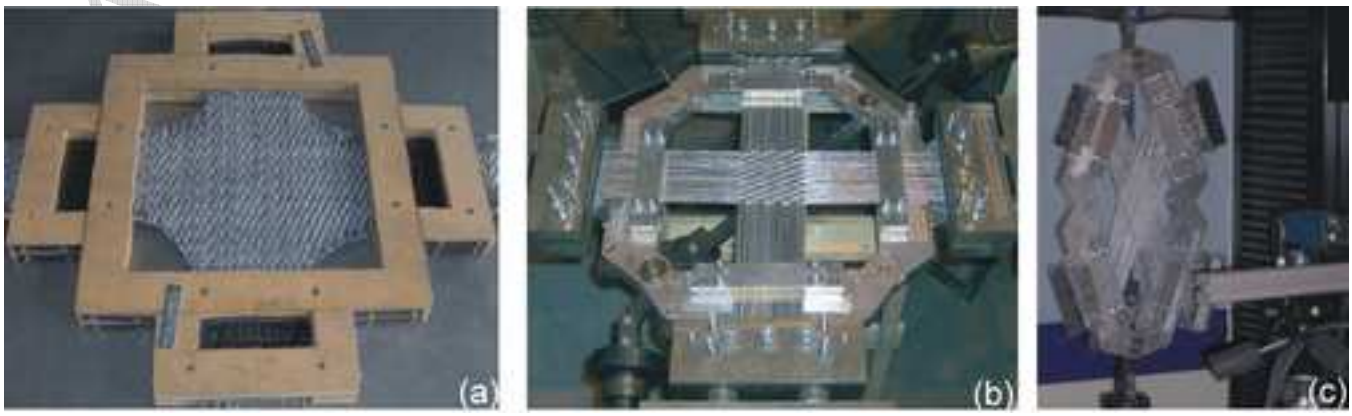

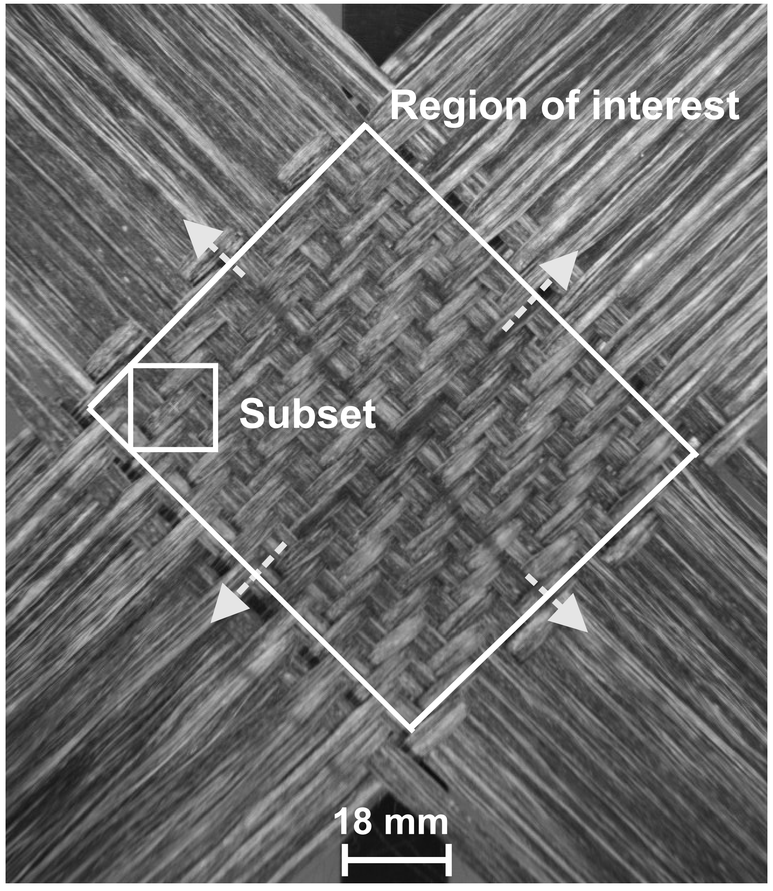

(a)

(b)

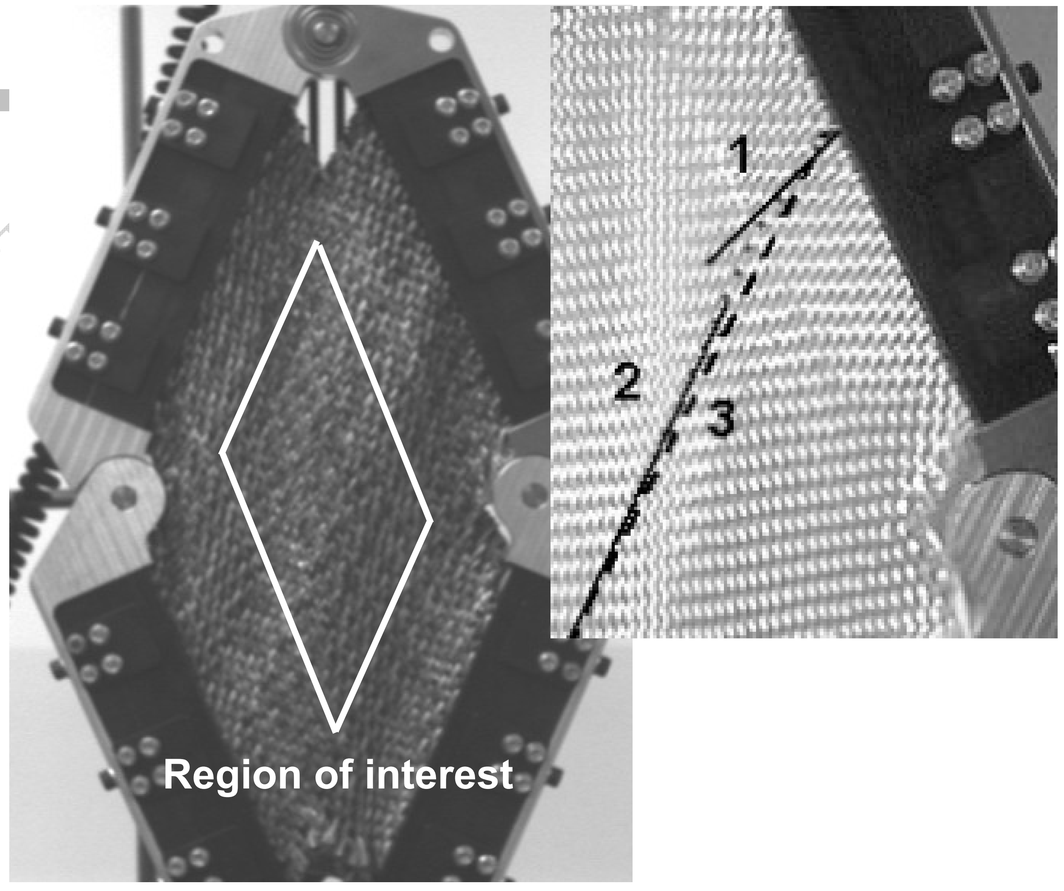

(c)

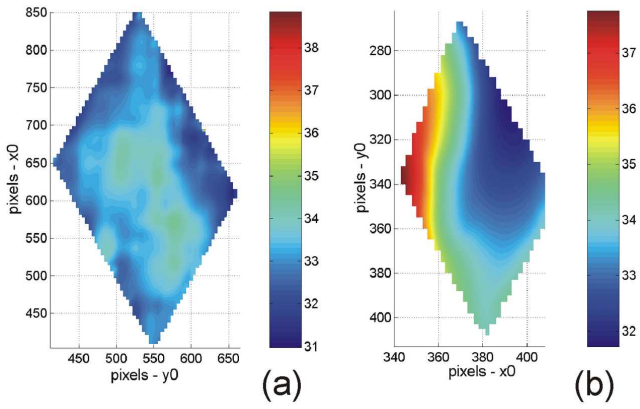

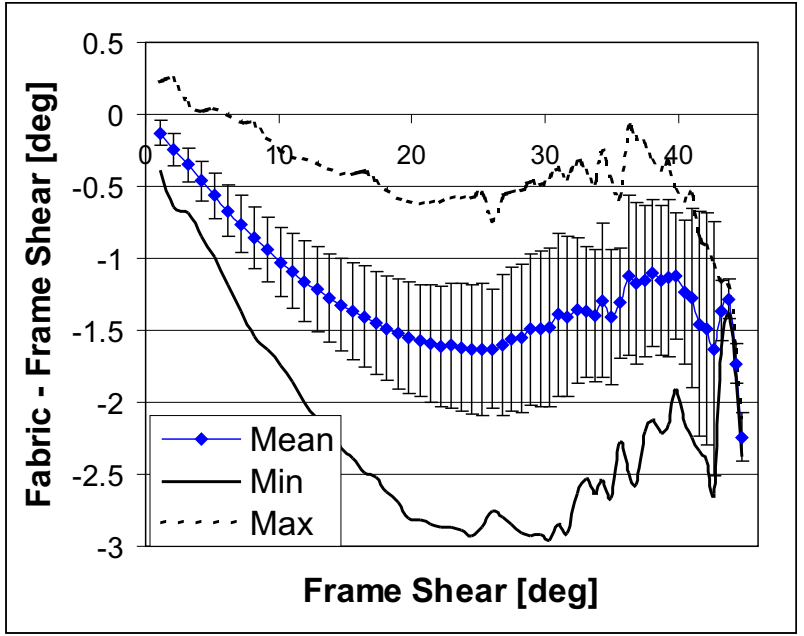

R580

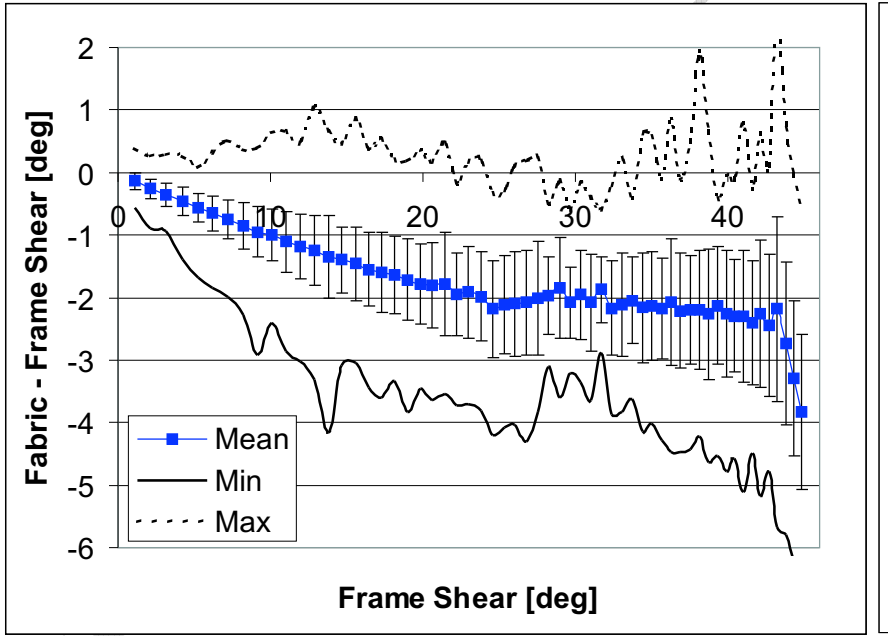

B2 - 0/90

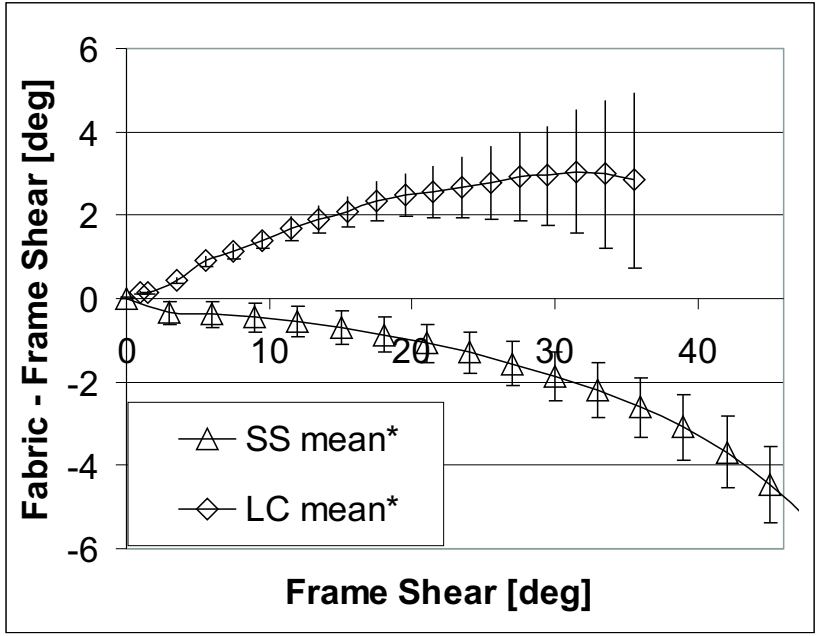

RR2

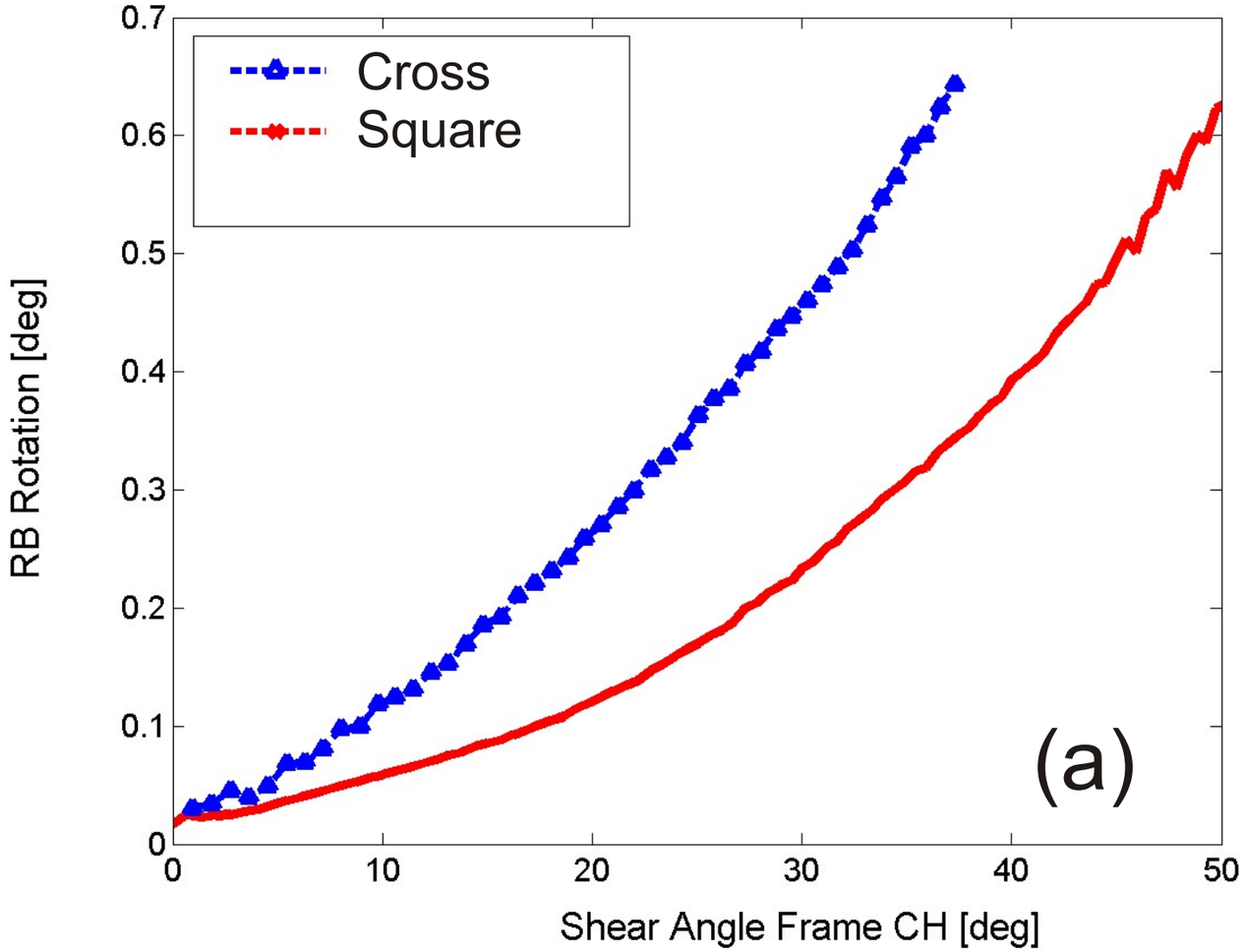
Cross
Square
RB Rotation [deg]
Shear Angle Frame CH [deg]
0
0.1
0.2
0.3
0.4
0.5
0.6
0.7
0
10
20
30
40
50
(a)

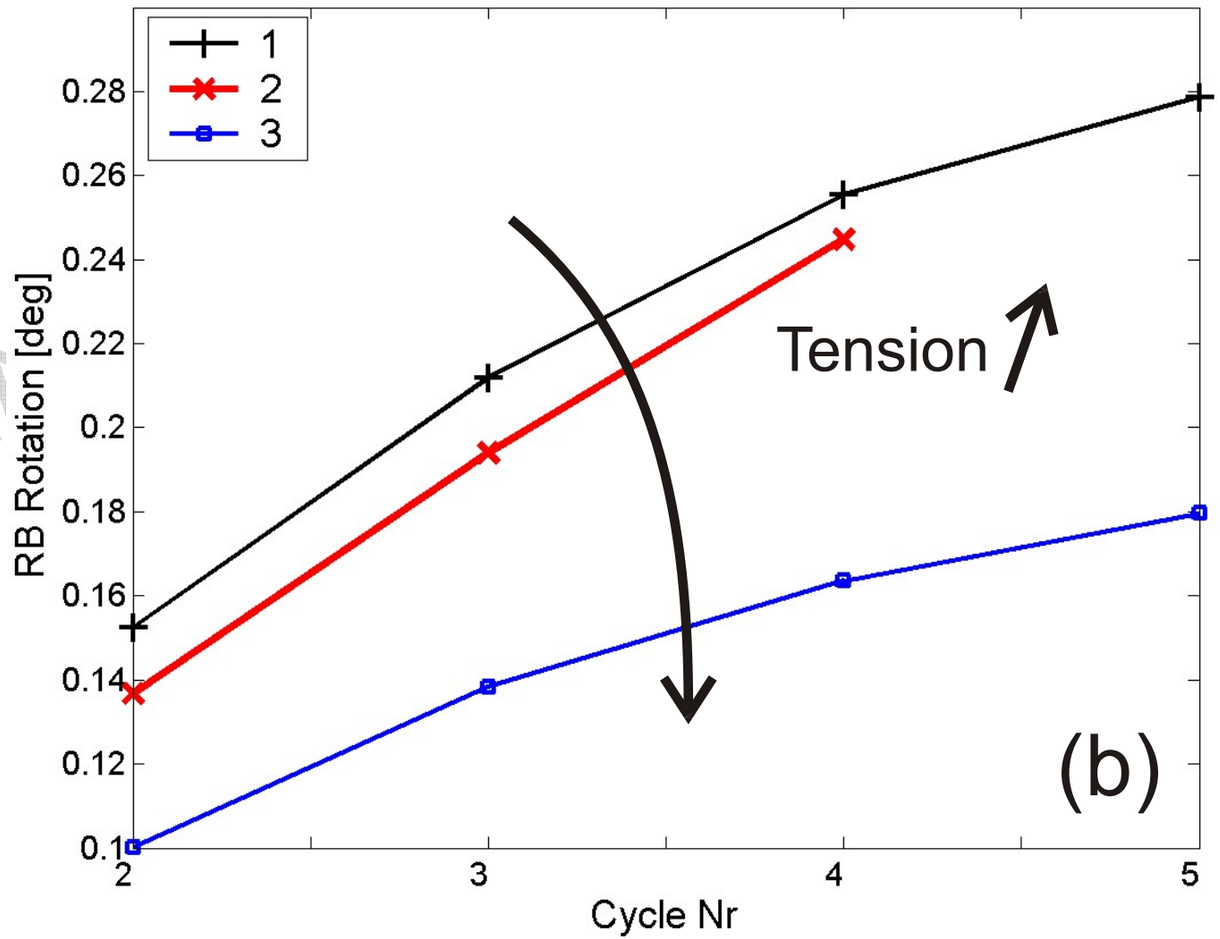
1
2
3
RB Rotation [deg]
Cycle Nr
Tension
0.1
0.12
0.14
0.16
0.18
0.2
0.22
0.24
0.26
0.28
2
3
4
5
(b)

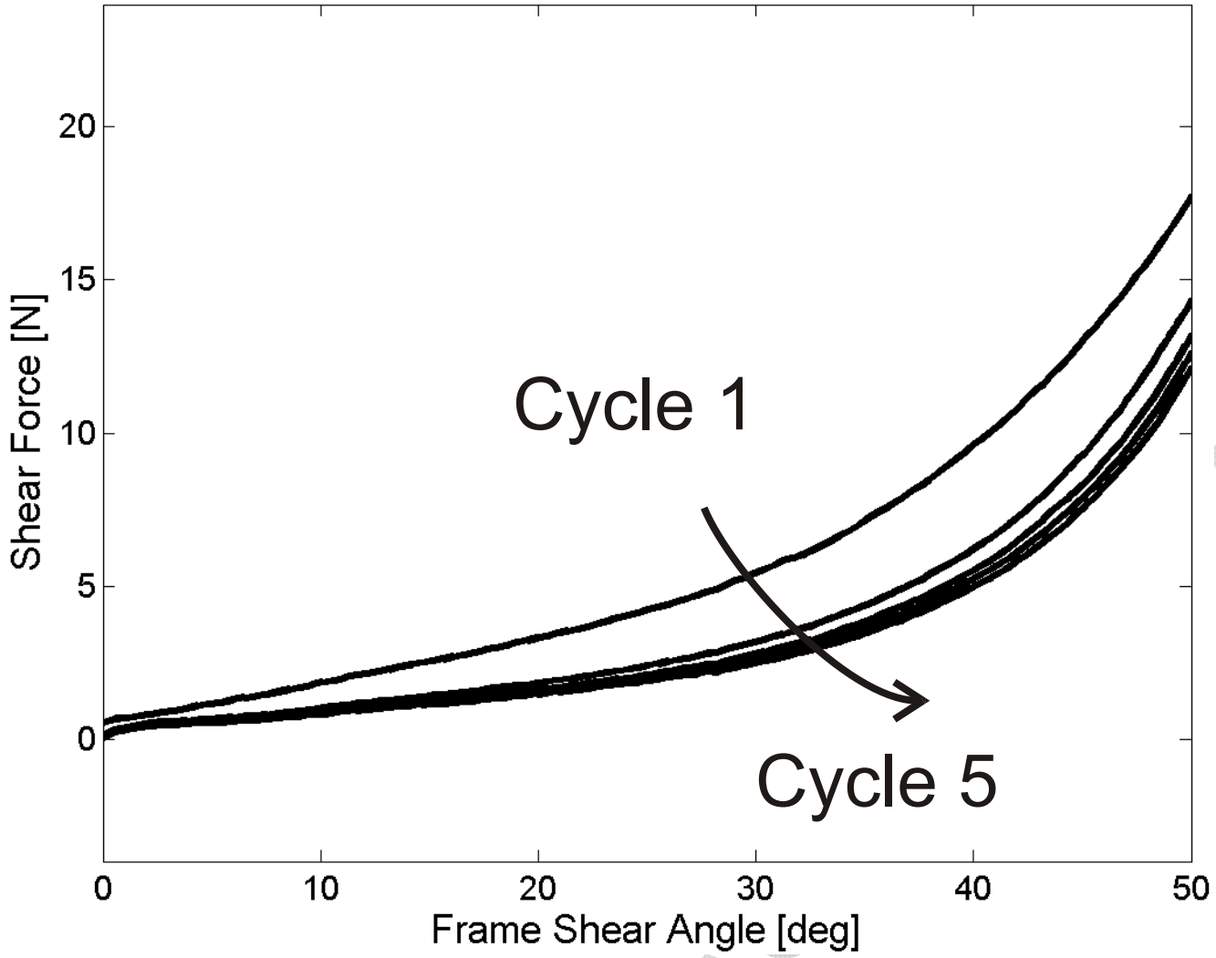
Shear Force [N]
Frame Shear Angle [deg]
Cycle 1
Cycle 5
0
5
10
15
20
0
10
20
30
40
50

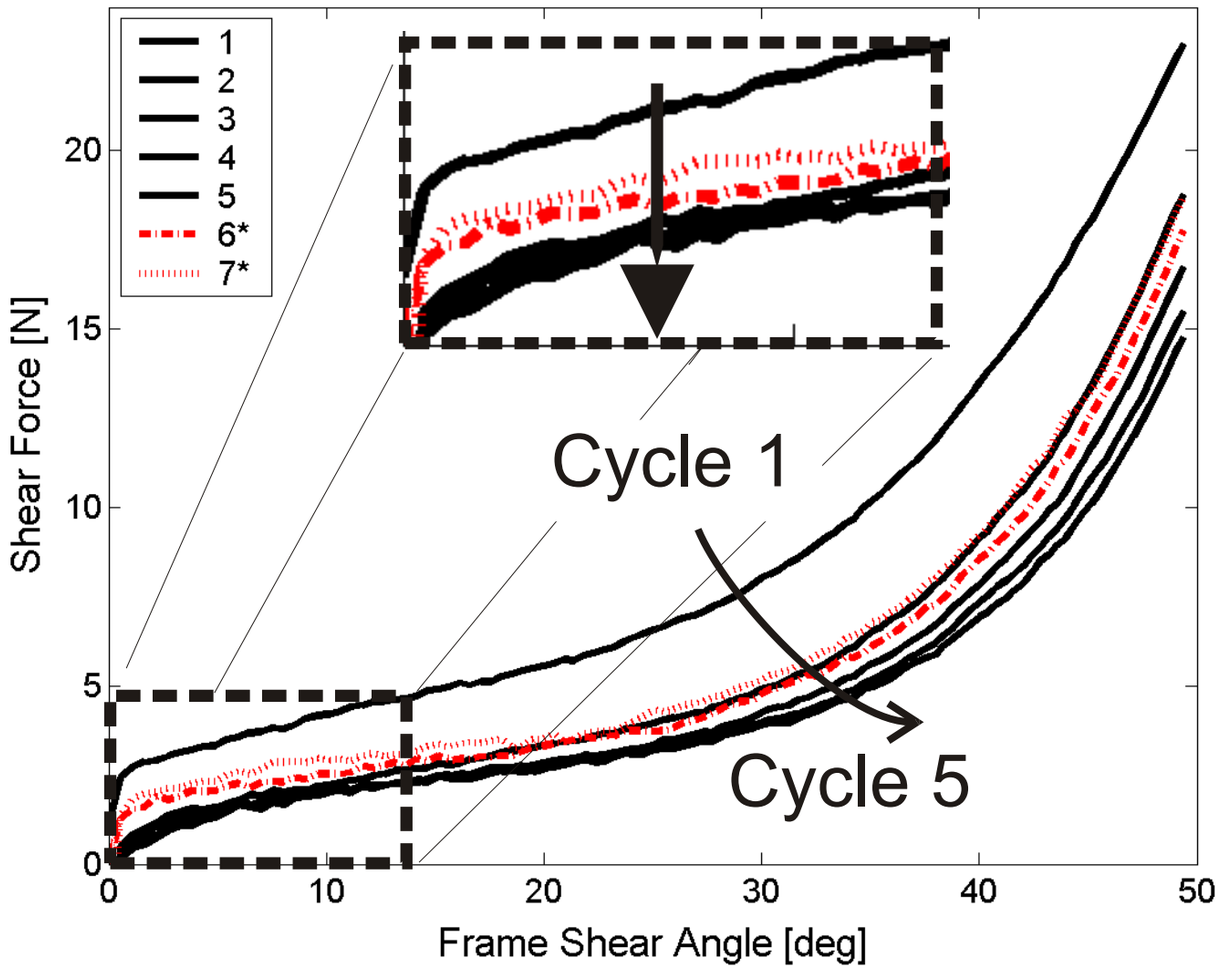
1
2
3
4
5
6*
7*
Shear Force [N]
Frame Shear Angle [deg]
Cycle 1
Cycle 5
0
5
10
15
20
0
10
20
30
40
50

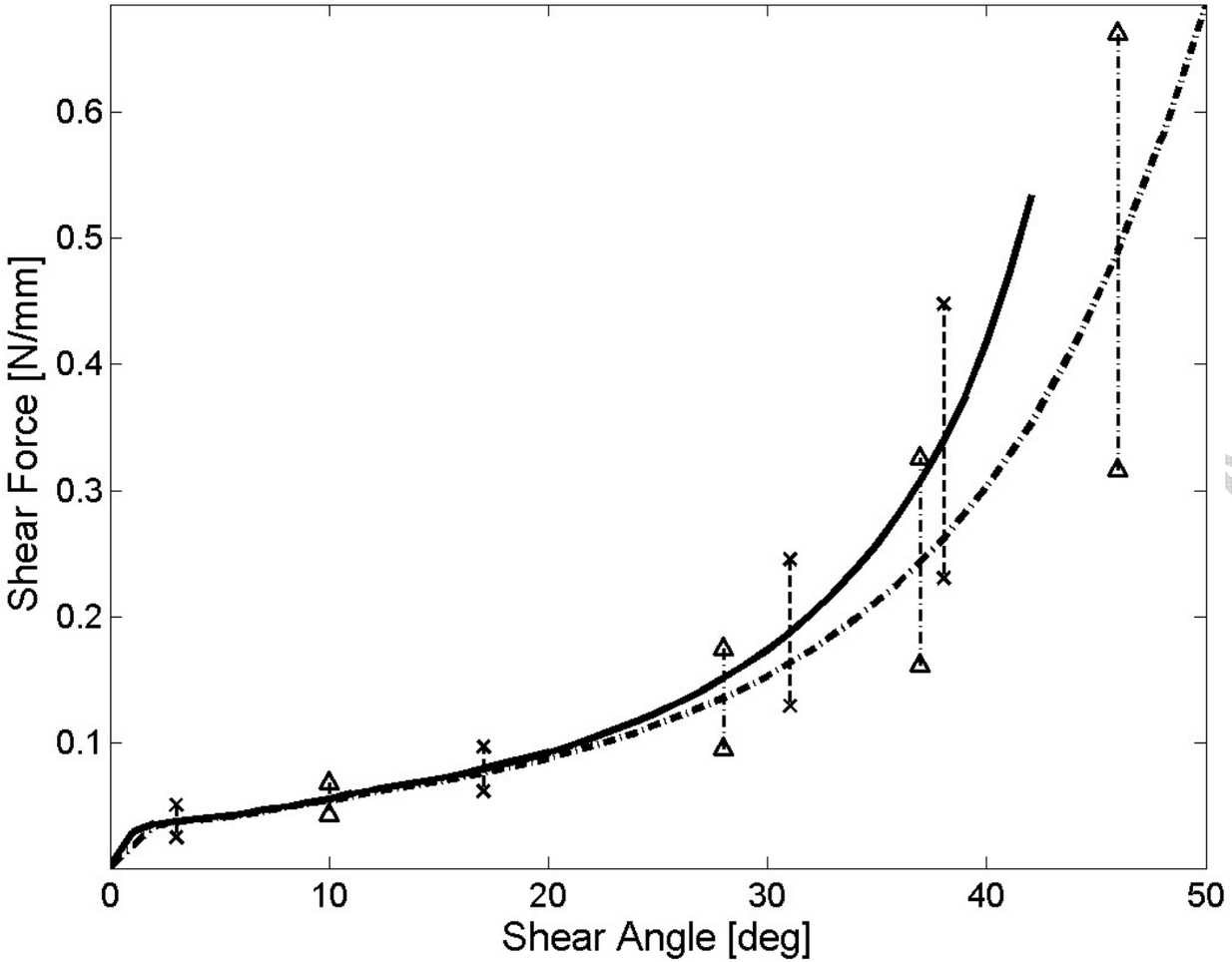
Shear Force [N/mm]
Shear Angle [deg]
0
0.1
0.2
0.3
0.4
0.5
0.6
10
20
30
40
50

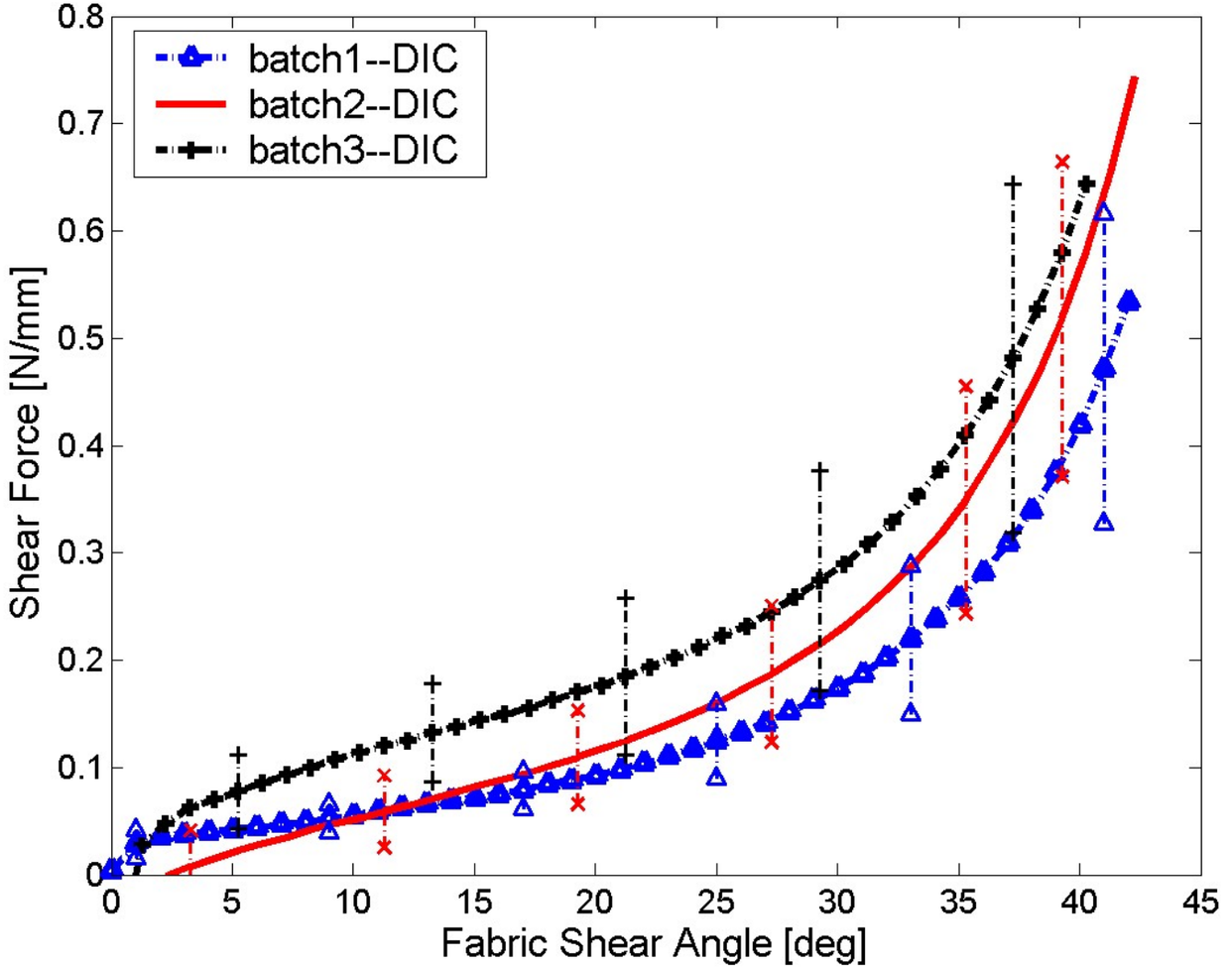
batch1--DIC
batch2--DIC
batch3--DIC
Shear Force [N/mm]
Fabric Shear Angle [deg]
0
0.1
0.2
0.3
0.4
0.5
0.6
0.7
0.8
5
10
15
20
25
30
35
40
45

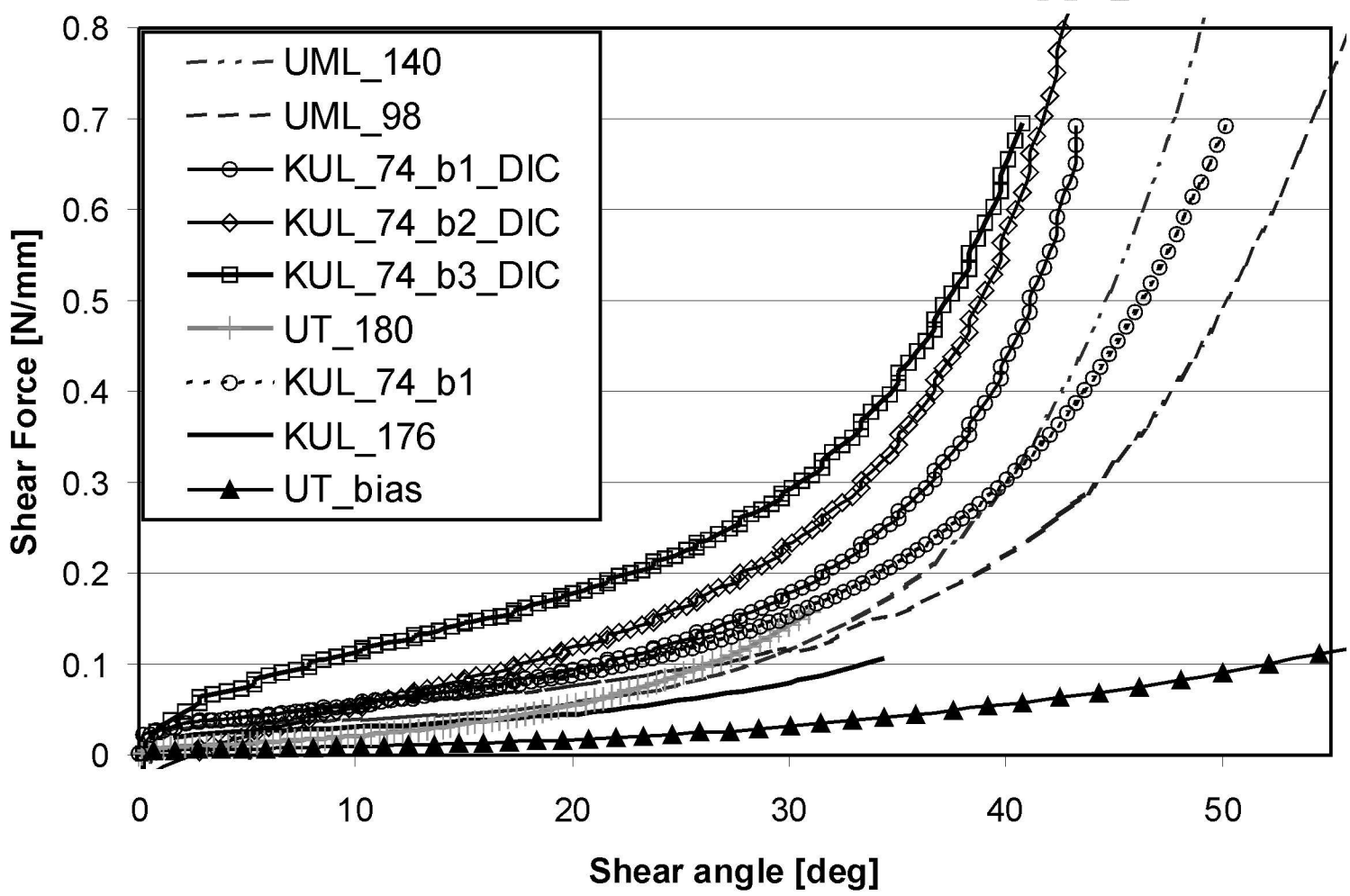
UML_140
UML_98
KUL_74_b1_DIC
KUL_74_b2_DIC
KUL_74_b3_DIC
UT_180
KUL_74_b1
KUL_176
UT_bias
Shear Force [N/mm]
0.8
0.7
0.6
0.5
0.4
0.3
0.2
0.1
0
0
10
20
30
40
50
Shear angle [deg]

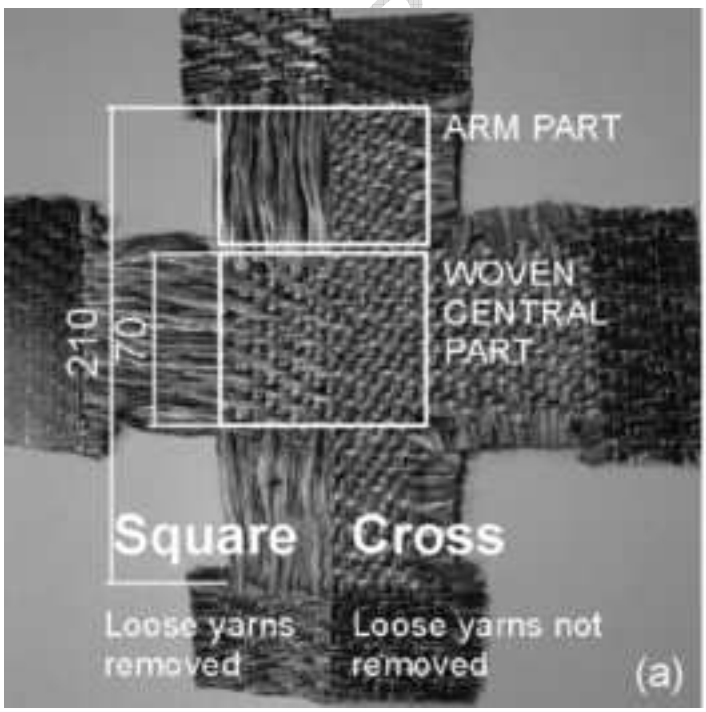

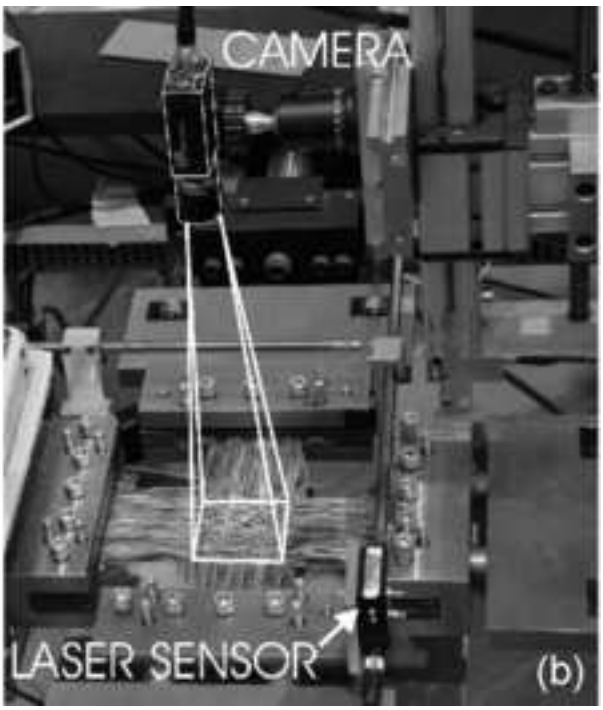

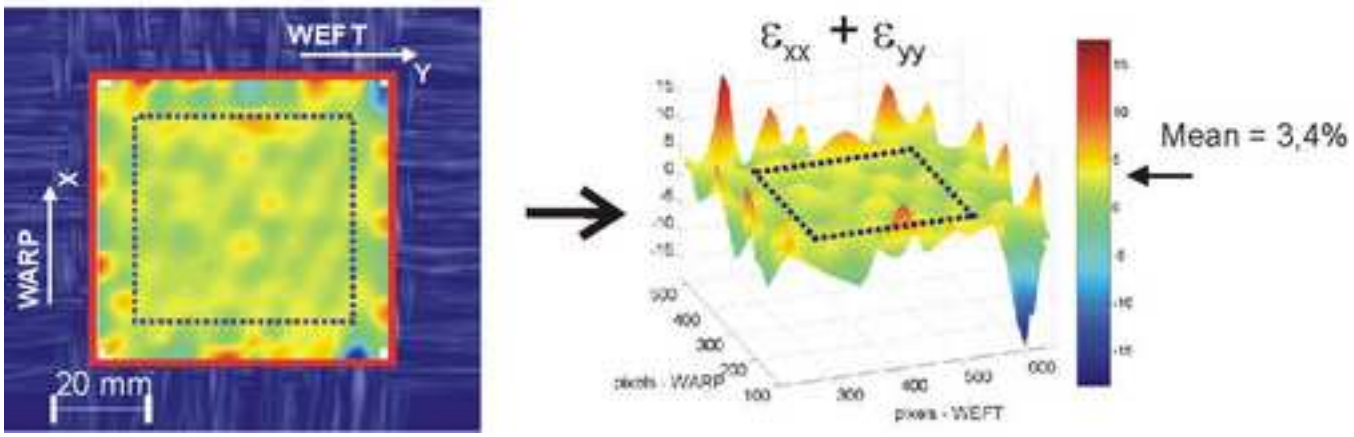

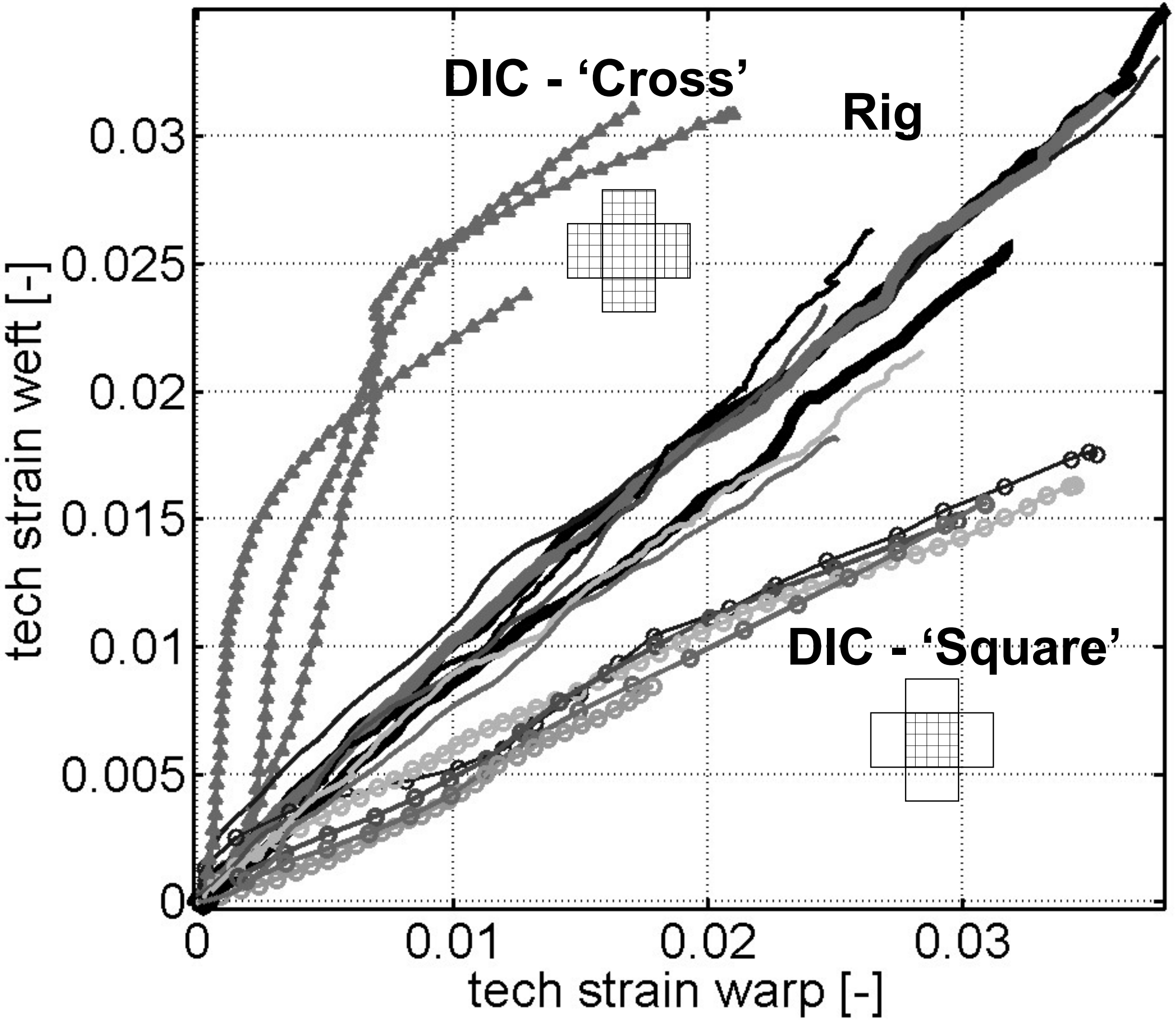
DIC - ‘Cross’
Rig
DIC - ‘Square’
tech strain weft [-]
tech strain warp [-]
0
0.005
0.01
0.015
0.02
0.025
0.03
0
0.01
0.02
0.03

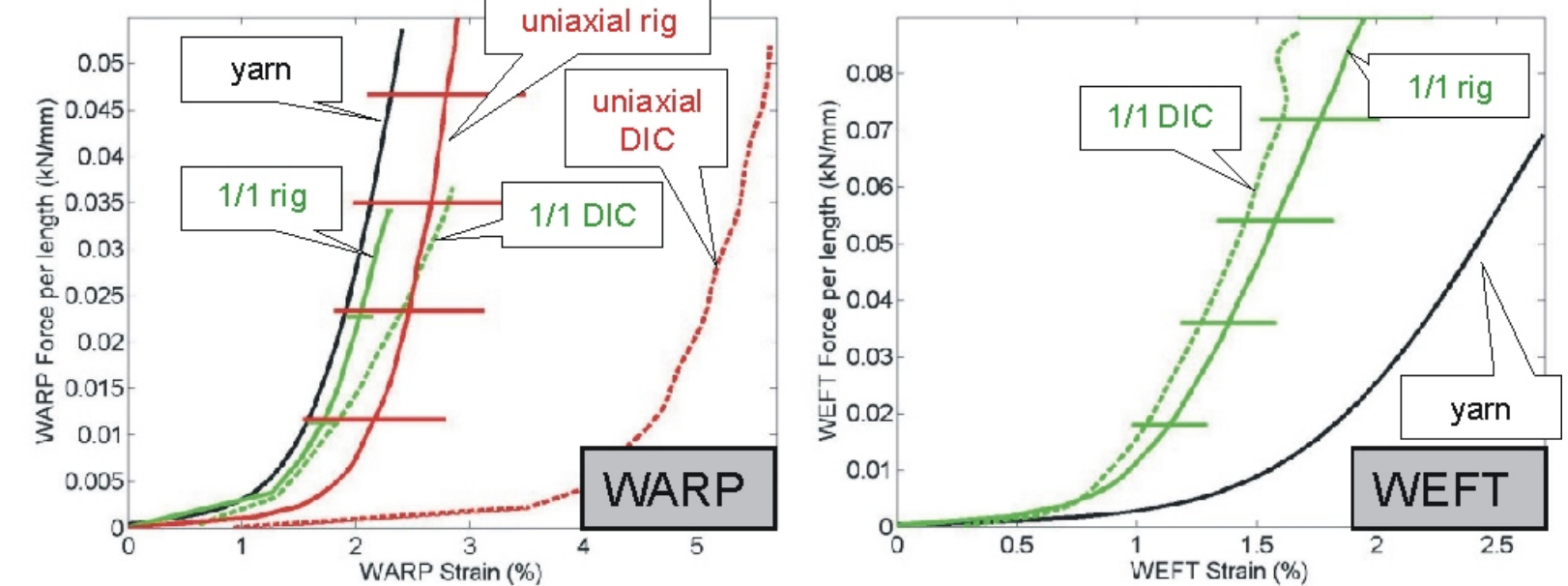
yarn
uniaxial rig
uniaxial DIC
1/1 rig
1/1 DIC
WARP
WARP Force per length (kN/mm)
WARP Strain (%)
0.05
0.045
0.04
0.035
0.03
0.025
0.02
0.015
0.01
0.005
0
0
1
2
3
4
5
1/1 DIC
1/1 rig
yarn
WEFT
WEFT Force per length (kN/mm)
WEFT Strain (%)
0.08
0.07
0.06
0.05
0.04
0.03
0.02
0.01
0
0
0.5
1
1.5
2
2.5